

Effect of novel ternary ligand system on acidic electroless Ni–P plating on AZ91D magnesium alloy

Hui-long WANG, Ling-yun LIU, Wen-feng JIANG

School of Chemistry, Dalian University of Technology, Dalian 116023, China

Received 30 August 2013; accepted 16 January 2014

Abstract: The electroless Ni–P coatings on AZ91D magnesium alloy substrate were prepared using the acidic hypophosphite-reduced electroless nickel bath containing the novel ternary ligand system. The results indicate that the deposition rate varies with the ternary ligand concentration in plating solution. The structural and morphological characteristics of the coatings were analyzed by XRD and SEM. The anticorrosion properties of the Ni–P coatings were evaluated in 3.5% NaCl solution by electrochemical impedance and potentiodynamic polarization methods. The amount of ternary ligands in electroless plating bath has an significant effect on the surface morphology and structure of Ni–P coatings. The decrease of crystallization temperature and increase of crystallization heat of all the deposits with an increase in ternary ligand concentration are found by DSC measurements. The coating obtained with 0.035 mol/L ternary ligand additive in plating bath can offer a better surface homogeneity and improve corrosion resistance.

Key words: ligand; electroless deposition; Ni–P coating; magnesium alloy

1 Introduction

Magnesium alloys have been widely used in the aerospace, automobile, electronics fields because of its various merits, such as low density, high specific strength and a relatively high stiffness [1,2]. However, the further applications of magnesium and its alloys are restricted for several reasons, among which one is the relatively poor corrosion and wear resistance [3–5]. Strategies that have been investigated to address this obstacle include chemical conversion, anodization, electroless plating, PVD, laser cladding and so on [6–15]. Amongst a variety of attempts, the electroless deposition of Ni–P alloy coating on magnesium alloy substrate has attracted special interest due to its excellent corrosion and wear resistance, good uniformity, solderability and surface lubricity [16–18]. As a special autocatalytic chemical reduction process, the electroless nickel deposition processes are very complex. The characteristics and properties of electroless Ni–P coatings are strongly determined by the compositions of the plating solutions [19,20]. Formulations of electroless

plating baths are in general multi-component systems comprising at least one or more ligands. The ligands included in bath can reduce the concentration of free nickel ions and prevent the precipitation of nickel phosphate, thus increasing the bath stability [21,22]. Evidence suggests that the type and structure of ligands in electroless plating bath play a critical role in determining deposition rate, precipitation equilibrium point of nickel phosphite, phosphorus content and corrosion resistance of Ni–P coatings. The effect of ligand on the morphology, microstructure and properties of Ni–P coatings has been studied [23,24] and the optimum mole ratio of ligand to nickel was found to be 0.33 (Ligand to Ni=1:3) [19]. The complexing agents used in electroless Ni–P plating process are mainly focused on single-ligand system at the present time. However, formulations of electroless plating baths should satisfy the multi-requirements in electroless Ni–P plating process, such as appropriate deposition rate, lower plating temperature, good bath stability and high corrosion resistance in practice. The electroless plating baths containing single-ligand system make the requirements mentioned above more difficult to achieve.

There is still a lack of reports on bath formulations containing mixed-ligand system. And also studies on the effect of mixed-ligand system on electroless deposited Ni–P alloys on AZ91D magnesium alloy are rather limited.

In this work, the bath containing ternary ligand system for electroless Ni–P plating on AZ91D magnesium alloy was developed. The effects of ternary ligand system on the deposition rate, structure and properties of electroless Ni–P coatings were also investigated.

2 Experimental

2.1 Sample preparation

AZ91D magnesium alloys containing 9.0%Al, 0.68%Zn, 0.26%Mn, 0.04%Si, 0.02%Cu, 0.004%Fe, 0.001%Ni and the remainder Mg were used as the substrate material. The substrate materials were abraded gradually to 1500 grade with silicon carbide grit paper, ultrasonically cleaned in acetone for degreasing, washed with distilled water, and dried in dry air. Then, the samples of dimensions 30 mm×20 mm×2 mm were suspended on Nylon wire and immersed in an alkaline solution, containing 50 g/L sodium hydroxide and 10 g/L sodium phosphate at (65±5) °C for 10 min, then etched in a solution of chromic and nitric acids for a duration of 45 s, subsequently activated in a 40% (v/v) HF solution for 10 min. The samples were rinsed with distilled water after every step of the pretreatment process. Following the pretreatment stage, the samples were immersed in electroless bath for plating. The composition and operation conditions of electroless plating Ni–P are as follows: nickel sulfate hexahydrate 20 g/L, sodium hypophosphite 20 g/L, hydrofluoric acid (40% v/v) 12 mL/L, ammonium bifluoride 10 g/L, thiourea 1 mg/L, 2-mercapto-benzo-thiosole 0.25 mg/L, sodium dodecyl sulfate 0.15 g/L. The used Ni–P plating bath solution contained ternary ligand system including citric acid as a main ligand, glycine and alanine as accessorial ligands. The mass ratio of ternary ligand system based on theoretical calculation is equal to 7:3:1 for citric acid, glycine, alanine. The total ligand concentrations in the Ni–P plating bath range from 0.005 to 0.05 mol/L. The initial pH value of the plating bath was adjusted by ammonia solutions to 5.4±0.2. The temperature of the plating bath was controlled within (80±1) °C using a digitally controlled thermostat. The stability of the bath containing the ternary ligand system was evaluated by using accelerated PdCl₂ test [25]. The stability time of the bath was found to be 4850 s, which is superior to that of the common used electroless Ni–P plating bath containing the single citric acid ligand in the same concentration (~2000 s).

2.2 Characterization

2.2.1 Gravimetric method

The plating rate was determined by gravimetric method and was expressed in terms of the mass gain during the deposition process. The plating rate was calculated from the following equation:

$$v = \frac{10^4 \Delta m}{\rho S t} \quad (1)$$

where v is the plating rate; Δm is the mass gain; S is the surface area of specimen; ρ is the density of the deposit; and t is the plating duration.

2.2.2 XRD and SEM studies

The X-ray diffraction (XRD) patterns of the prepared coating samples were made in as-plated condition with a computer controlled Rigaku D/max–2000 powder diffractometer using Cu K α radiation (30 kV, 30 mA) with a scan rate of 5 (°)/min for structural and grain size evaluation. Scanning electron microscope (SEM, QUANTA 450, FEI) with EDX (energy dispersive X-ray spectroscopy) attachment was used to determine the surface morphology and elemental composition of the coatings.

2.2.3 Thermal stability studies

The crystallization and phase transformation behavior of the coating samples was studied with a differential scanning calorimeter (DSC, Q20, USA) in the temperature range of 300–450 °C at a heating rate of 10 °C/min under argon environment with a flow rate of 40 mL/min.

2.2.4 Electrochemical corrosion measurements

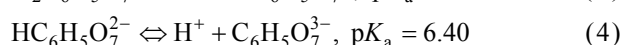
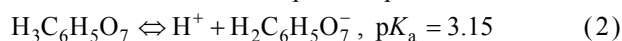
The electrochemical corrosion measurements were performed using CorrTest electrochemical work station (CS310, Wuhan CorrTest Instrument Co. Ltd.) coupled to a computer, and the test system was controlled and experimental data were recorded by the CorrTest software package. A conventional three-electrode glass cell, with the sample with an exposed area of 1 cm² as the work electrode (WE), the saturated calomel electrode (SCE) as the reference electrode (RE) and platinum foil as the auxiliary electrode, was employed. A non-deaerated 3.5% NaCl solution maintained at (25±1) °C was used as the aggressive solution. Prior to the beginning of the electrochemical corrosion measurements the sample was immersed in the corrosive medium for about 30 min to establish the steady state potential. The electrochemical impedance spectroscopy (EIS) measurements were carried out for corrosion potential at sinusoidal voltage excitation with perturbation amplitude of 10 mV in a frequency range from 100 kHz to 0.01 Hz. All the recorded impedance diagrams were given in the Nyquist and Bode representations. After EIS measurements, the system was allowed for 30 min to reach its steady open circuit

potential (φ_{OCP}). The potentiodynamic polarization tests of samples were performed successively at a scan rate of 0.8 mV/s in the applied potential range from -250 mV to 750 mV with respect to φ_{OCP} . The electrochemical parameters such as corrosion potential φ_{corr} , corrosion current density J_{corr} , Tafel slopes B_c and B_a and polarization resistance R_p , were calculated using the Tafel extrapolation method. The working electrode was cleaned in acetone and rinsed with deionized water before the electrochemical test.

3 Results and discussion

3.1 Effect of ternary ligand system on deposition rate

Experiments were carried out to investigate the influence of ligand concentration on the deposition rate (Fig. 1). It can be found that the deposition rate increases with an increase in ternary ligand concentration from 0.005 to 0.02 mol/L, beyond which the deposition rate starts to decrease, indicating the highest deposition rate occurring in the bath containing 0.02 mol/L ternary ligands. The main ligand citric acid in aqueous solution exists in four forms that depend on pH value of solution.



The fraction of each form of citric acid against pH can be calculated on the basis of the corresponding $\text{p}K_a$ value and the results are presented in Fig. 2. Clearly, $\text{HC}_6\text{H}_5\text{O}_7^{2-}$ is the dominant species over the pH range from 5.0 to 6.0. Reports in Ref. [26] suggest that in mildly acidic conditions citric acid can react with nickel ions to produce stable $\text{Ni}(\text{HC}_6\text{H}_5\text{O}_7)$ complex that illustrates a 1:1 complex ratio and $\lg K$ value of 5.11. Glycine and alanine as the accessorial ligands in the bath can also combine with nickel ions to give stable ligand–nickel complexes [27]. When the concentration of ternary ligands is less than 0.020 mol/L, the ternary ligand system in the bath can maintain the electroless Ni–P plating solution stable, but cannot convert all aquo-nickel ions into complexes. Also, the main ligand citric acid with certain reducing property would facilitate the reduction of nickel ions, resulting in an increased deposition rate within the range of ternary ligand concentration from 0.005 to 0.020 mol/L. A further increase in ternary ligand concentration, however, may cause an increase in stability of the bath and decrease in reduced property of nickel ions and thus reduce the deposition rate [28]. The deposition rate is an important process control parameter in electroless Ni–P plating, both too fast or too slow deposition rate being unfavorable for high quality deposits. Hence, the ternary ligand concentration of 0.035 mol/L is selected in this experiment.

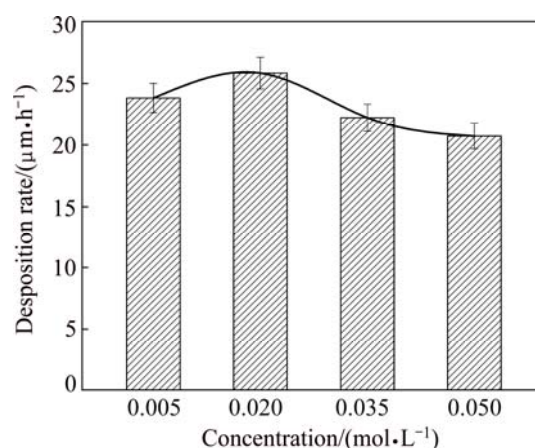


Fig. 1 Dependence of Ni–P deposition rate on ternary ligand concentration in bath

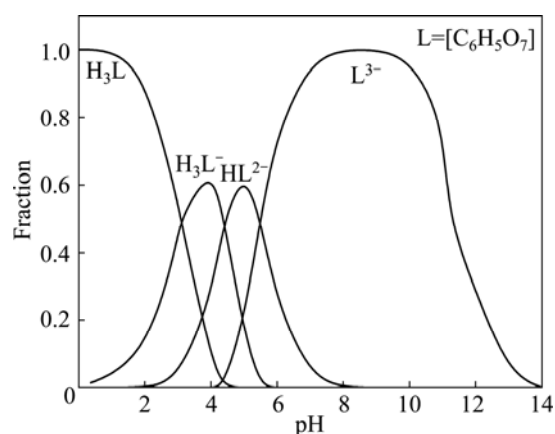


Fig. 2 Variation of citric acid species with pH

3.2 Effect of ternary ligand system on morphology and structure of coatings

The surface morphology of the electroless Ni–P coatings obtained from the baths with various ternary ligand concentrations is given in Fig. 3. Although all the coatings exhibit a similar spherical nodular structure, changes in ternary ligand concentration affect the surface morphology of the samples to some degree. The coating, obtained from the bath with lower ternary ligand concentration (0.005 mol/L), shows higher porosity and pores are located primarily on surface and at boundaries of the nodules (Fig. 3(a)). The observed high porosity of the coating is caused by the poor stability of the bath in the process of electroless Ni–P plating. The coarse nodular structure can be observed in Fig. 3(b) for the sample obtained in plating bath containing 0.02 mol/L ternary ligands. This can be interpreted as acceleration in deposition rate. Figure 3(c) shows a very smooth and dense surface with excellent uniformity and no apparent defects can be observed. The coating quality is not improved significantly with further increase in ternary ligand concentration (Fig. 3(d)). The results indicate that

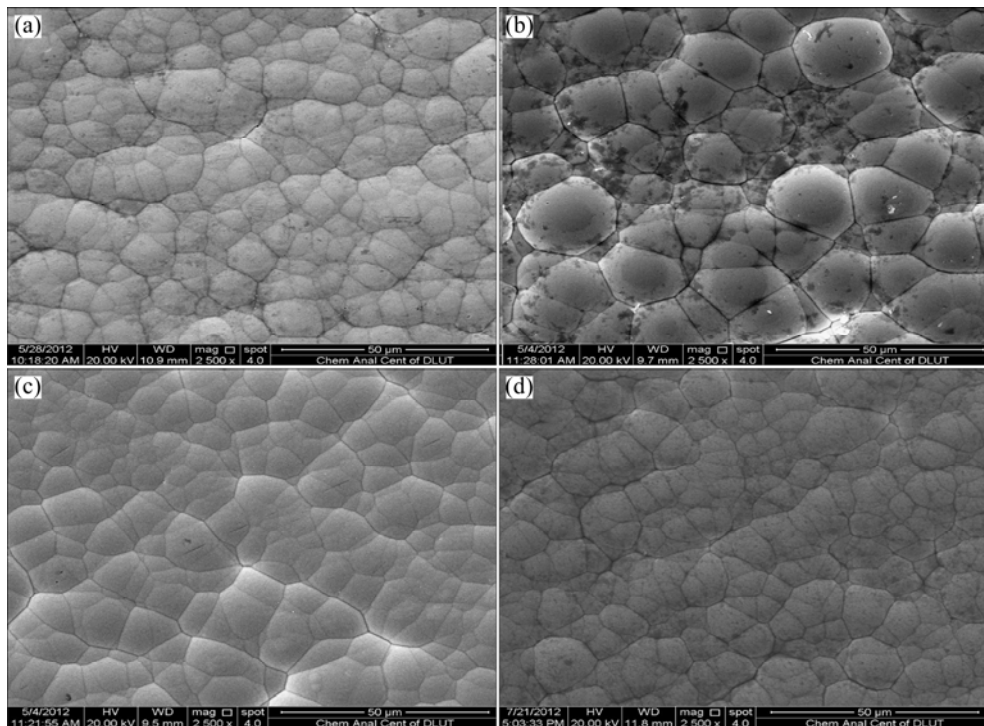


Fig. 3 SEM micrographs of electroless Ni-P coatings obtained from baths with various ternary ligand concentrations: (a) 0.005 mol/L; (b) 0.020 mol/L; (c) 0.035 mol/L; (d) 0.050 mol/L

the amount of ternary ligands in the bath has an important influence on the surface morphology of the prepared Ni-P coatings. An optimum ternary ligand concentration (0.035 mol/L) in the bath is necessary for obtaining high quality Ni-P coatings on magnesium alloy substrates. Figure 4 gives EDX spectra for the Ni-P coating obtained from the bath with 0.035 mol/L ternary ligands. From the spectra, the presence of Ni and P in the coating is evident. The phosphorus and nickel contents in the Ni-P coating were determined to be 8.69% and 91.31% by EDX analysis, respectively. When the phosphorus content is in medium level, the electroless as-deposited Ni-P plating has a mixture microstructure of amorphous and nanocrystalline nickel [29].

In order to compare the influence of various ligand systems on morphology and structure of the Ni-P coatings, SEM micrograph of electroless Ni-P coating obtained from the bath with 0.035 mol/L citric acid is presented in Fig. 5. It is clear that the Ni-P coating obtained in plating bath containing citric acid as the single ligand shows large nodular structure with irregular grain boundaries, which can be attributed to the fast reduction of Ni^{2+} ions and poor stability of the formed Ni^{2+} -citric acid complexes [30]. The result shows that the electroless Ni-P coatings obtained from the baths with the ternary ligand system are superior to those obtained from the baths with the single ligand system.

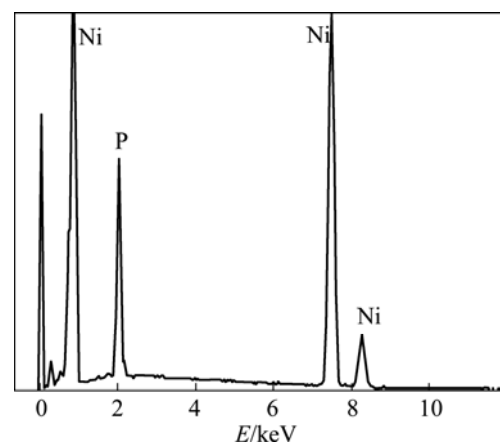


Fig. 4 EDX spectrum of as-plated Ni-P coating

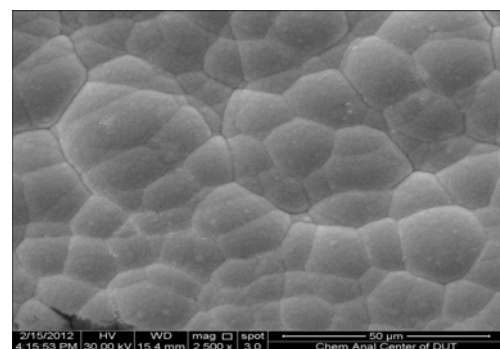


Fig. 5 SEM micrograph of electroless Ni-P coating obtained from bath with 0.035 mol/L citric acid

Figure 6 shows the XRD patterns of the electroless Ni–P coatings obtained from the baths with different ternary ligand concentrations. All the coatings exhibit broad and high intensity diffraction at about 45° that can be ascribed to the (111) plane of a face centered cubic (FCC) phase of nickel, indicating that the coatings have an amorphous structure possibly with microcrystalline areas. The electroless Ni–P deposition process is based on a redox reaction in which nickel and phosphorus atoms are co-deposited on the surface of the substrate. According to the explanation given by BALARAJU et al [31], the amorphous structure of the Ni–P coatings is mainly a consequence of difference in atomic radius between nickel ($r_{\text{Ni}}=1.62 \text{ \AA}$) and phosphorus ($r_{\text{P}}=1.23 \text{ \AA}$). The different atomic sizes between Ni and P can result in crystal lattice deformation when phosphorus atoms are incorporated into crystal lattice of nickel, which permits the formation of a crystalline structure only over a limited distance. The average size of nanocrystalline phase in the different samples can be determined by applying the Scherrer equation on the Ni (111) diffraction peaks:

$$D = \frac{K\lambda}{\beta \cos \theta} \quad (5)$$

where D is the average crystalline size, K is the constant, λ is the wavelength of the X-ray radiation, β is the corrected band broadening (full width at half maximum (FWHM)) after subtraction of equipment broadening, and θ is the diffraction angle. The calculated average nanocrystalline phase sizes for samples obtained from the baths containing 0.005, 0.020, 0.035 and 0.050 mol/L ternary ligands are 54, 52, 44, and 41 nm, respectively. It is known that the crystalline phase size and crystallinity of coatings are directly related. Therefore, the experimental results show that the crystallinity of Ni–P coatings decreases with an increase in the concentration of ternary ligands in the bath.

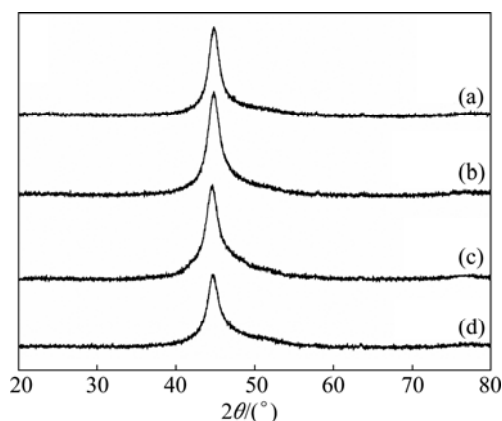


Fig. 6 XRD patterns of electroless Ni–P coatings obtained from baths with different ternary ligand concentrations: (a) 0.005 mol/L; (b) 0.020 mol/L; (c) 0.035 mol/L; (d) 0.050 mol/L

3.3 Effect of ternary ligand system on thermal stability of coatings

The DSC curves of the samples, obtained from the baths with different ligand concentrations, are presented in Fig. 7. The thermal profile indicates that all the samples exhibit a well-defined exothermic peak. The observed exothermic peak is due to the occurrence of the crystallization of Ni–P amorphous alloy and the formation of Ni_3P phase at high temperature around 400 °C [32]. The samples obtained from the baths containing 0.005, 0.020, 0.035 and 0.050 mol/L ternary ligands show the exothermic peak at 407.24, 401.14, 400.16 and 399.48 °C, respectively. The calculated heats released in the crystallization and phase transformation processes for the samples mentioned above are 29.88, 33.51, 38.88 and 39.20 J/g, respectively. Within the range of ternary ligand concentration from 0.005 to 0.05 mol/L, the observed decrease in crystallization temperature and increase in released heat in the process of crystallization may be due to the influence of nanocrystalline phases in Ni–P coatings. The nanocrystalline phase with highly ordered structure is more stable than the amorphous matrix which has a disordered structure. The relatively stable nanocrystalline phases in Ni–P coatings inhibit the movement and rearrangement of some nickel or phosphorus atoms in the amorphous matrix, so these disorder atoms need higher temperature to perform the crystalline process [24]. According to the results obtained in section 3.2 in the present work, the crystallinity of Ni–P coatings decreases with an increase in ternary ligand concentration in plating solution. As a result, the crystallization temperature decreases, and the released heat increases with an increase in ternary ligand concentration from 0.005 to 0.050 mol/L in the baths.

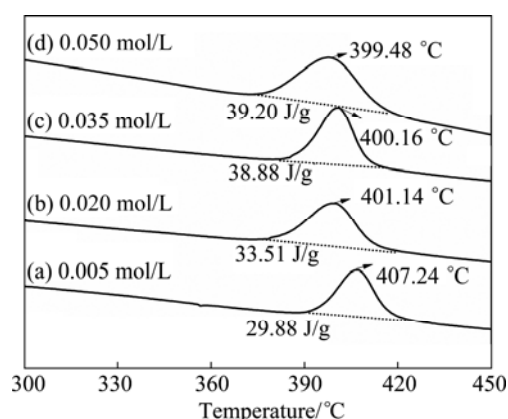


Fig. 7 DSC curves of electroless Ni–P coatings obtained from baths with different ternary ligand concentrations

3.4 Effect of ternary ligand system on corrosion resistance of coatings

3.4.1 Electrochemical impedance spectroscopy (EIS) study

Electrochemical impedance spectroscopy method is one of the powerful techniques to investigate the corrosion resistance of Ni–P coatings on AZ91D magnesium alloy. The Ni–P coating samples obtained from the baths containing 0.005, 0.020, 0.035 and 0.050 mol/L ternary ligands are denoted as NP1, NP2, NP3 and NP4, respectively. Figures 8 and 9 present the Nyquist and Bode plots obtained for different Ni–P coatings immersed in 3.5% NaCl solution at their respective open circuit potentials. The Nyquist plots appear to be similar for all the samples, exhibiting only one capacitive loop in the high frequency region. This signifies that a charge transfer process mainly controls the corrosion of the samples in NaCl solution. Although all the Nyquist plots appear to be similar with respect to their shapes, they differ appreciably in the diameter of the loops. This indicates that the corrosion resistance of the samples in the corrosive medium is different from each other even with the same corrosion mechanisms. The capacitive loop diameters can be used to calculate the impedance value. The bigger the capacitive loop diameter, the better the corrosion resistance of the coating. From the Nyquist plots, one can conclude that

the corrosion resistance is decreased in the order of NP1<NP2<NP4< NP3. The Ni–P coating, obtained with 0.035 mol/L ternary ligand additive exhibits the best corrosion protective ability among all the samples. Bode plots of different coatings seen in Fig. 9 show a single-phase angle maximum in the plot of lg *f* versus phase angle. In all the coatings it is almost 90° signifying pure capacitive behavior which confirms that only a single time constant is involved in the corrosion reaction process. The Bode plots of NP3 reveal higher impedance and broader phase angle than other prepared samples, which could be ascribed to the excellent corrosion resistance of NP3 coating.

An equivalent electrical circuit model shown in Fig. 10 has been used to simulate the metal-solution interface and to fit experimental data for the samples, where a constant phase element (CPE) is parallel to the charge transfer resistance of coatings (*R_c*) and both of which are in series with the solution resistance (*R_s*). Considering the rough surface of the coatings, a CPE was used instead of a capacitor to account for non-homogeneity and deviations of the value of physical property in the system. The CPE can be defined by CPE-T and CPE-P [33]. The CPE can be expressed as

$$Z = \frac{1}{T\sqrt{\omega^P}} \tag{6}$$

where ω is angular frequency of the AC signal, *T* is capacitance and *P* is nonhomogeneity constant. Depending on the value of *P*, CPE can represent resistance when *P*=0, capacitance when *P*=1 and Warburg impedance when *P*=0.5. The parameters of equivalent circuit were evaluated using Zview software and the results are presented in Table 1. Comparing the obtained data, it can be observed that NP3 is of the highest value of charge transfer resistance and the lowest value of the constant phase element (CPE-T) among all the prepared samples, which shows a better corrosion

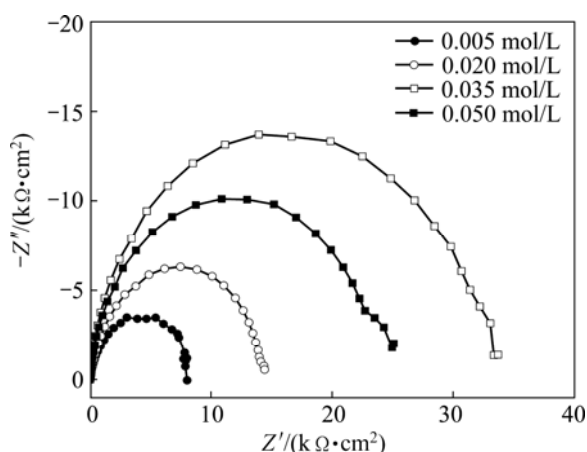


Fig. 8 Nyquist plots for electroless Ni–P coatings obtained from baths with different ternary ligand concentrations

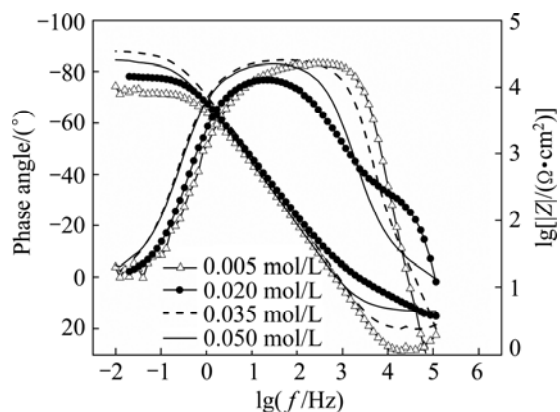


Fig. 9 Bode plots electroless Ni–P coatings obtained from baths with different ternary ligand concentrations

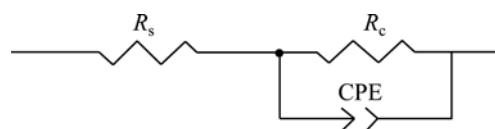


Fig. 10 Equivalent electrical circuit for modeling EIS data

Table 1 Electrochemical parameters calculated from EIS data of samples immersed in 3.5% NaCl solution

Sample	<i>R_s</i> / (Ω·cm ²)	<i>T</i> / (μF·cm ⁻²)	<i>P</i>	<i>R_c</i> / (Ω·cm ²)
NP1	1.375	28.91	0.94887	7486
NP2	5.425	35.18	0.83541	15133
NP3	2.437	21.20	0.95511	31397
NP4	4.487	28.72	0.93130	23776

protective ability and a denser structure than NP1, NP2 and NP4 [34]. The higher CPE-P value of NP3 sample confirms the better surface homogeneity of the NP3 coating. These observations are consistent with SEM measurements.

3.4.2 Potentiodynamic polarization studies

The corrosion behaviors of the prepared coatings immersed in 3.5% NaCl solution were also investigated by potentiodynamic polarization method. Figure 11 shows the potentiodynamic curves of the samples in 3.5% NaCl solution. The electrochemical corrosion parameters derived from the potentiodynamic polarization curves are listed in Table 2. Clearly, the potentiodynamic curves for all the Ni–P coatings seem to be similar, oxygen reduction reaction dominating the cathodic sides and active reaction dominating the anodic sides. In comparison with the potentiodynamic curves of the Ni–P coatings, the corrosion potential of NP3 is more positive than that of NP1, NP2 or NP4 and the anodic dissolution reaction of NP3 was restrained significantly, verifying better corrosion resistance of NP3 coating. Values of corrosion current densities obtained for various Ni–P coatings in 3.5% NaCl solution follow the order of NP1>NP2>NP4>NP3, which is in a good matching with results obtained from EIS measurements.

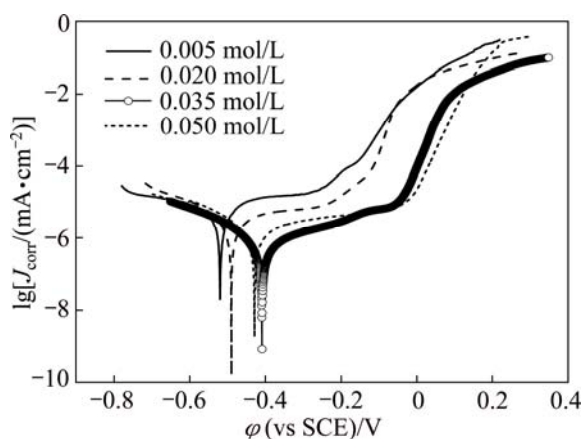


Fig. 11 Potentiodynamic curves of electroless Ni–P coatings obtained from baths with different ternary ligand concentrations

Table 2 Electrochemical polarization parameters of various samples immersed in 3.5% NaCl solution

Sample	$\phi_{\text{corr}}/\text{V}$	$J_{\text{corr}}/(\mu\text{A}\cdot\text{cm}^{-2})$	B_a/mV	B_c/mV	$R_p/(\Omega\cdot\text{cm}^2)$
NP1	-0.5194	2.340	93.73	64.13	6976
NP2	-0.4895	1.230	85.47	68.67	12633
NP3	-0.3865	0.557	80.54	72.22	26487
NP4	-0.4289	0.612	87.75	67.27	24277

Corrosion protective ability of electroless Ni–P coatings mainly depends on phosphorus content and the porosity of the coatings [31]. The phosphorus contents in the NP1, NP2, NP3 and NP4 were determined to be 7.16%, 7.35%, 8.69% and 8.71% by EDXS analysis, respectively. According to the literature report on Ni–P coatings, the preferential dissolution of nickel results in the accumulation of phosphorus, which favors the formation of Ni–P stable intermediate compounds and adsorbed hypophosphite anions on the surface layer [31]. The produced Ni–P compounds are considered to act as barrier passive film and the adsorbed hypophosphite anions will in turn block the supply of water to the coating surface and prevent the hydration of nickel. So, the increase in the amount of phosphorus present in coatings strengthens the corrosion resistance of the Ni–P coatings in 3.5% NaCl solution. SEM micrographs of the as-plated electroless Ni–P coatings also prove that NP3 has denser and more compact structure compared with other three samples, resulting in better corrosion protection ability of NP3 sample.

4 Conclusions

Electroless Ni–P coatings on AZ91D magnesium alloy substrate were prepared by using acidic ternary ligand system based hypophosphite-reduced electroless nickel bath. The ternary ligand system in the bath can affect the deposition rate, surface morphology and microstructure, thermal stability and corrosion resistance of electroless Ni–P coatings. By adjusting the amount of ternary ligands in electroless plating bath, the optimum deposition rate of electroless Ni–P plating and high quality coatings consisting of a mixture of amorphous and nanocrystalline phase can be obtained. The crystallization temperature decreases and heat released in the crystallization and phase transformation processes for the Ni–P coatings increases with an increase in ternary ligand concentration in plating solution. Electrochemical corrosion studies show that the Ni–P coating obtained with 0.035 mol/L ternary ligand additive in plating bath can provide better surface homogeneity and superior corrosion resistance in 3.5% NaCl solution.

References

- [1] GU C D, LIAN J S, LI G Y, NIU L Y, JIANG Z H. Electroless Ni–P plating on AZ91D magnesium alloy from a sulfate solution [J]. *Journal of Alloys and Compounds*, 2005, 391(1–2): 104–109.
- [2] LIU Z M, GAO W. Electroless nickel plating on AZ91 Mg alloy substrate [J]. *Surface and Coatings Technology*, 2006, 200(16–17): 5087–5093.

- [3] LI J Z, TIAN Y W, HUANG Z Q, ZHANG X. Studies of the porosity in electroless nickel deposits on magnesium alloy [J]. *Applied Surface Science*, 2006, 252(8): 2839–2846.
- [4] GRAY J E, LUAN B. Protective coatings on magnesium and its alloys—A critical review [J]. *Journal of Alloys and Compounds*, 2002, 336(1–2): 88–113.
- [5] ZHU L Q, SONG G L. Improved corrosion resistance of AZ91D magnesium alloy by an aluminium-alloyed coating [J]. *Surface and Coatings Technology*, 2006, 200(8): 2834–2840.
- [6] CHEN Jun, SONG Ying-wei, SHAN Da-yong, HAN En-hou. Properties of dawsonite conversion film on AZ31 magnesium alloy [J]. *Transactions of Nonferrous Metals Society of China*, 2011, 21(4): 936–942.
- [7] HUO H W, LI Y, WANG F H. Corrosion of AZ91D magnesium alloy with a chemical conversion coating and electroless nickel layer [J]. *Corrosion Science*, 2004, 46(6): 1467–1477.
- [8] ZENG R C, LAN Z D, KONG L H, HUANG Y D, CUI H Z. Characterization of calcium-modified zinc phosphate conversion coatings and their influences on corrosion resistance of AZ31 alloy [J]. *Surface and Coatings Technology*, 2011, 205(11): 3347–3355.
- [9] HSIAO H Y, TSAI W T. Characterization of anodic films formed on AZ91D magnesium alloy [J]. *Surface and Coatings Technology*, 2005, 190(2–3): 299–308.
- [10] SHARMA A K, SURESH M R, BHOJRAJ H, NARAYANAMURTHY H, SAHU R E. Electroless nickel plating on magnesium alloy [J]. *Metal Finishing*, 1998, 96(3): 10–16.
- [11] CHEN Jun, ZENG Rong-chang, HUANG Wei-jiu, ZHENG Zi-qing, WANG Zhen-lin, WANG Jun. Characterization and wear resistance of macro-arc oxidation coating on magnesium alloy AZ91 in simulated body fluids [J]. *Transactions of Nonferrous Metals Society of China*, 2008, 18(S): s361–s364.
- [12] SHIGEMATSU I, NAKAMURA M, SAITOU N, SHIMOJIMA K. Surface treatment of AZ91D magnesium alloy by aluminum diffusion coating [J]. *Journal of Materials Science Letters*, 2000, 19(6): 473–475.
- [13] LIU Feng, SHAN Da-yong, SONG Ying-wei, HAN En-hou. Formation process of composite plasma electrolytic oxidation coating containing zirconium oxides on AM50 magnesium alloy [J]. *Transactions of Nonferrous Metals Society of China*, 2011, 21(4): 943–948.
- [14] ZENG R C, CHEN J, KUANG J, ZHANG J. Influence of silane on corrosion resistance of magnesium alloy AZ31 with thermally sprayed aluminum coating [J]. *Rare Metals*, 2010, 29(2): 193–197.
- [15] JUN Y, SUN G P, LIU C, JIA S Q, FANG S J, JIA S S. Characterization and wear resistance of laser surface cladding AZ91D alloy with Al+Al₂O₃ [J]. *Journal of Materials Science*, 2007, 42(10): 3607–3612.
- [16] ZHAO Q, LIU Y. Electroless Ni–Cu–P–PTFE composite coatings and their anticorrosion properties [J]. *Surface and Coatings Technology*, 2005, 200(7): 2510–2514.
- [17] NOVAK M, VOJTECH D, NOVA P, VITU T. Tribological properties of heat-treated electroless Ni–P coatings on AZ91 alloy [J]. *Applied Surface Science*, 2011, 257(23): 9982–9985.
- [18] GOU Yin-ning, HUANG Wei-jiu, ZENG Rong-chang, ZHU Yi. Influence of pH values on electroless Ni–P–SiC plating on AZ91D magnesium alloy [J]. *Transactions of Nonferrous Metals Society of China*, 2010, 20(S): s674–s678.
- [19] AMBAT R, ZHOU W. Electroless nickel-plating on AZ91D magnesium alloy: Effect of substrate microstructure and plating parameters [J]. *Surface and Coatings Technology*, 2004, 179(2–3): 124–134.
- [20] WINOWLIN JAPPES J T, RAMAMOORTHY B, KESAVAN NAIR P. A study on the influence of process parameters on efficiency and crystallinity of electroless Ni–P deposits [J]. *Journal of Materials Processing Technology*, 2005, 169(2): 308–313.
- [21] NWOSU N, DAVIDSON A, HINDLE C, BARKER M. On the influence of surfactant incorporation during electroless nickel plating [J]. *Industrial and Engineering Chemistry Research*, 2012, 51(1): 5635–5644.
- [22] JIN Y, YU H Y, YANG D J, SUN D B. Effects of complexing agents on acidic electroless nickel deposition [J]. *Rare Metals*, 2010, 29(4): 401–406.
- [23] HUANG Y S, CUI F Z. Effect of complexing agent on the morphology and microstructure of electroless deposited Ni–P alloy [J]. *Surface and Coatings Technology*, 2007, 201(9–11): 5416–5418.
- [24] CHENG Y H, ZOU Y, CHENG L, LIU W. Effect of complexing agents on properties of electroless Ni–P deposits [J]. *Materials Science and Technology*, 2008, 24(4): 457–460.
- [25] EL-REHIM S S A, SHAFFEI M, EL-IBIARI N, HALEM S A. Effect of additives on plating rate and bath stability of electroless deposition of nickel–phosphorus–boron on aluminum [J]. *Metal Finishing*, 1996, 94(1): 29–33.
- [26] NIU Zhen-jiang, YU Ping, WANG Fei-hua, LI Ze-lin, WU Ting-hua. Effects of citric acid on electroless Ni–P alloy deposition rate and properties [J]. *Electroplating and Finishing*, 2003, 22(5): 23–26. (in Chinese)
- [27] YUAN Jin, ZHONG Hui-min, LI Cong. Synthesis and analysis of Ni²⁺-amino acid complexes [J]. *Amino Acids & Biotic Resources*, 1995, 17(3): 40–42. (in Chinese)
- [28] WANG H L, LIU L Y, DOU Y, ZHANG W Z, JIANG W F. Preparation and corrosion resistance of electroless Ni–P/SiC functionally gradient coatings on AZ91D magnesium alloy [J]. *Applied Surface Science*, 2013, 286: 319–327.
- [29] ZHANG W X, HUANG N, HE J G, JIANG Z H, JIANG Q, LIAN J S. Electroless deposition of Ni–W–P coating on AZ91D magnesium alloy [J]. *Applied Surface Science*, 2007, 253(11): 5116–5121.
- [30] HARI KRISHNAN K, JOHN S, SRINIVASAN K N, PRAVEEN J, GANESAN M, KAVIMANI P M. An overall aspect of electroless Ni–P depositions—A review article [J]. *Metallurgical and Materials Transactions A*, 2006, 37(6): 1917–1926.
- [31] BALARAJU J N, EZHIL SELVI V, WILLIAM GRIPS V K, RAJAM K S. Electrochemical studies on electroless ternary and quaternary Ni–P based alloys [J]. *Electrochimica Acta*, 2006, 52(3): 1064–1074.
- [32] SONG J Y, YU J. Residual stress measurements in electroless plated Ni–P films [J]. *Thin solid films*, 2002, 415(1–2): 167–172.
- [33] JEON M K, WON J Y, OH K S, LEE K R, WOO S I. Performance degradation study of a direct methanol fuel cell by electrochemical impedance spectroscopy [J]. *Electrochimica Acta*, 2007, 53(2): 447–452.
- [34] SONG Y W, SHAN D Y, HAN E H. Comparative study on corrosion protection properties of electroless Ni–P–ZrO₂ and Ni–P coatings on AZ91D magnesium alloy [J]. *Materials and Corrosion*, 2007, 58(7): 506–510.

新型三元复合络合剂体系对 AZ91D 镁合金 表面酸性化学镀 Ni-P 的影响

王慧龙, 刘凌云, 姜文凤

大连理工大学 化学学院, 大连 116023

摘 要: 利用含新型三元复合络合剂的酸性化学镀镍液体系, 在 AZ91D 镁合金表面通过化学镀制备 Ni-P 防护镀层。结果表明, 镀层沉积速率随着镀液中三元复合络合剂浓度的变化而改变。利用 X 射线衍射 (XRD)、扫描电子显微镜 (SEM) 和差热分析 (DSC) 对镀层结构、形貌以及热稳定性进行表征和分析。通过交流阻抗 (EIS) 和动电位扫描极化曲线对 Ni-P 镀层在 3.5% NaCl 溶液中的耐蚀性能进行评价。镀液中三元复合络合剂的浓度对 Ni-P 镀层的结构与形貌有显著影响。Ni-P 镀层的热稳定性随着三元复合络合剂浓度的增加而降低。当镀液中三元复合络合剂浓度为 0.035 mol/L 时, 所制备的 Ni-P 镀层致密、均一, 在 3.5% NaCl 溶液中表现出良好的耐蚀性能。

关键词: 络合剂; 化学镀; Ni-P 镀层; 镁合金

(Edited by Xiang-qun II)